Assessment of Physics-Informed Neural Networks for the mechanical characterization of viscoplastic materials

T. Doca[1], P.G. Marques Flávio[1], L. Pupure[2]

[1]*Universidade de Brasília (UnB)*
Faculty of Technology, Campus Darcy Ribeiro, Brasilia, Brazil
doca@unb.br
[2]*Riga Technical University (RTU)*
Department of Structural Engineering, Kalku iela, Rīga, Latvia

Abstract. Recent works have introduced the concept of Physics-Informed Neural Networks (PINN), which are trained to solve supervised learning tasks while fulfilling laws of physics described by nonlinear partial differential equations. In this work, this approach is compared to established constitutive models that address viscoplastic material behaviour. The materials analysed are the Poly-lactic acid (PLA) and the Acrylonitrile Butadiene Styrene (ABS). Two constitutive models are studied: Mulliken-Boyce, and an enhanced Zapas' model for viscoplasticity. The finite element method is employed for the discretization of solids under frictional contact and large strains. The output of the numerical model is coupled to a PINN, which is trained to replicate the experimental data and to be compared to the results provided by the constitutive models. The objective of this assessment is to verify the benefits and liabilities of each method. The focus is given to the accurate representation of stress-strain and/or force-displacement relationships. Other features such as computational time and memory bandwidth are also assessed.

Keywords: PINN, Mechanical characterization, PLA, ABS.

1 Introduction

The search for better engineering materials requires a strenuous and repetitive process, which may entail: material synthesis, specimen preparation, standardized testing, validation, certification, prototype testing, application and monitoring. This process is time consuming, wasteful and expensive. The use of computational modelling often leads to a significant amount of additional information towards material development [1]. However, classical numerical modelling (e.g. finite element and boundary element models) can also be costly and limited, specially when dealing with severe loading conditions such as finite strains [2], wear [3] and fretting fatigue [4]. Moreover, the modelling of advanced materials, such as polymer blends and composites, can be particularly challenging [5].

The advent of Neural Networks (NNs) and its widespread use in data analysis and parameter determination has quickly established this tools as another relevant approach to material engineering. In general, NNs require a significant amount of data for an accurate estimation, and even this do not ensure that physical constraints will be fulfilled. However, the combination of reliable physical equations with a consistent machine learning procedure has led to the inception of Physics-Informed Neural Networks (PINNs) [6]. This approach was initially designed for the solution of differential partial equations, but it can be extended include the architecture enhancements based on physical constraints [7] and to solve boundary value problems in general [8].

In this assessment two problem configurations are addressed: the standard ASTM 638 [9] tensile test setup, and a sphere-to-flat indentation [10, 11]. The objective is to evaluate the advantages of employing a PINN to estimate stress-strain behaviour of viscoplastic materials under either tensile stress or compressive stress.

2 Methodology

The method contains four steps: i) Experimental tests for the acquisition of reliable data; ii) Numerical modeling of geometries, boundaries and loading conditions using the Finite Element method; iii) Constitutive modeling, and iv) Training of a PINN to be used for evaluation of mechanical behaviour and enhancement of numerical parameters. These steps are detailed in the following.

2.1 Experimental setup

The experimental tests are carried-out using a MTS 809 system, fitted with a 5 kN load cell. During all tests, a force versus displacement curve is registered. Each test is carried-out four times, to produce a robust data set.

For the tensile tests a displacement rate of 5 mm/min is applied until the fracture of the specimen is observed. The specimen has a total length of 166 mm, a gauge length of 50 mm and a thickness of 3.65 mm. A clip gauge extensometer is used for the measurement of the gauge length strain. The tensile test specimen has its lower grip zone fully restrained, while the top grip zone is assigned to a prescribed displacement of 5 mm/min.

For the sphere-to-flat indentation test, a tungsten carbide sphere with a 15 mm diameter is employed as indentation tool while a prismatic polymer specimen (width: 25 mm; length: 25 mm; thickness: 5 mm) is used as counterpart. A prescribed axial displacement of 0.5 mm/min is applied to drive the flat counterpart towards the fixed sphere until the desired normal contact force (200, 400 or 600 N) is achieved. Afterwards, a three-dimensional profile of the indentation mark is produced via confocal laser microscopy. The profiles are then used for measurements of the spherical cap's diameter and depth, which are then correlated to the stress/strain levels observed at that given load condition. The interested reader may find a detailed description of this testing method in [12].

2.2 Numerical setup

Both problems are modeled in Abaqus v6.14, a quasi-static loading condition is assumed and a symmetry condition is applied to the solids center-line to ensure alignment. Bodies are discretized using 4-noded linear hexahedron finite elements. The tensile specimen, the sphere and the flat specimen contain a total of 4440, 2922 and 1692 elements, respectively. A more refined discretization is used in the gauge length and contact interface. Frictional contact is considered in the sphere-to-flat interface. The contact constraints are enforced via Lagrange method and surface-to-surface segmentation. Depictions of the discretized solids and its restraints are given in Fig. 1a and Fig. 1b.

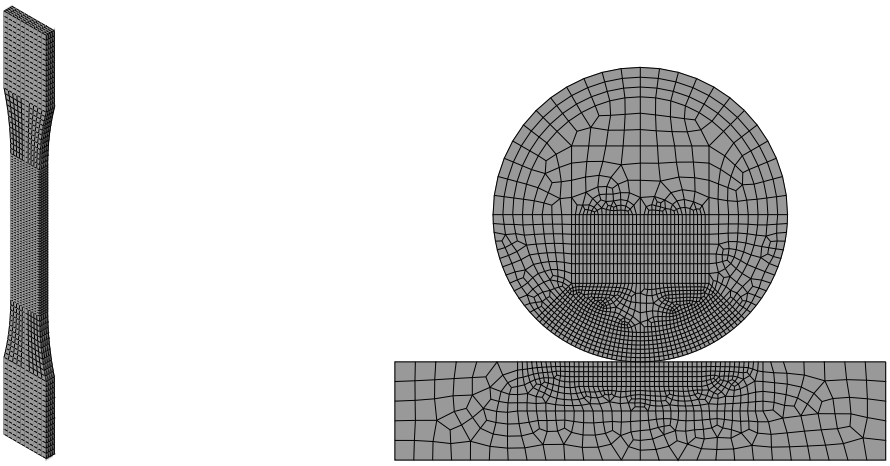

(a) Tensile specimen.

(b) XZ plane cut view of the sphere-to-flat setup.

Figure 1. Discretization of the geometries tested.

The prescribed displacement are applied following the experimental test procedures. The solution of the global stiffness system of equations, required for the determination of the nodal displacements, is carried-out using

the Newton method. The convergence criteria adopted for all simulations is a residual equal to 10^{-9}.

2.3 Material properties and Constitutive models

Two pure polymers have been chosen for this study: a Poly-lactic acid (PLA) and an Acrylonitrile Butadiene Styrene (ABS). These two materials have similar mechanical properties and are well known for having a distinct phase of viscoplastic behavior [13, 14], which deems them suitable options for this assessment. The constitutive models employed here are the Mulliken-Boyce [15] and an enhanced version of the Zapas-Crissman model for viscoplasticity [16] presented in [17]. Both models have been implemented as VUMAT subroutines that are coupled to the Abaqus FE model. The relevant properties, for the purposes of this study, are listed in Table 1.

Table 1. Relevant properties of PLA and ABS.

	PLA	ABS
Specific mass, ρ, (kg/m^3)	1240	1040
Elastic modulus, traction, E_t (MPa)	2500	2300
Elastic modulus, compression, E_c (MPa)	1650	1400
Poisson's coefficient, ν	0.39	0.38
Yield stress, traction, $\sigma_{y,t}$, (MPa)	45	21
Yield stress, compression, $\sigma_{y,c}$, (MPa)	90	40
Hardness, spherical indentation, HB, (MPa)	169	99
Friction coefficient, μ	0.19	0.23
Elastic modulus, alpha, E_α [MPa]	1422.6	1490.5
Elastic modulus, beta, E_β [MPa]	6.0	5.3
Pre-exponential factor, alpha, $\dot{\gamma}^p_{0,\alpha}$, $[s^{-1}]$	$2.82 \cdot 10^{16}$	$2.79 \cdot 10^{16}$
Pre-exponential factor, beta, $\dot{\gamma}^p_{0,\beta}$, $[s^{-1}]$	$3.31 \cdot 10^{5}$	$3.18 \cdot 10^{5}$
Pressure coefficient, alpha, $\alpha_{p,\alpha}$	0.162	0.165
Pressure coefficient, beta, $\alpha_{p,\beta}$	0.245	0.248
Activation energy, alpha, $\alpha_{p,\alpha}$, [J]	$3.5 \cdot 10^{-19}$	$4.0 \cdot 10^{-19}$
Activation energy, beta, $\alpha_{p,\beta}$, [J]	$3.6 \cdot 10^{-20}$	$3.6 \cdot 10^{-20}$
Softening slope, alpha, h_α, [MPa]	242	290
Preferred states of athermal shear strength, alpha, $s_{ss,\alpha}$, [MPa]	$0.62S_{0,\alpha}$	$0.88S_{0,\alpha}$
Ruberry modulus, C_r, [MPa]	14.1	11.9
Limiting chain extensibility, $\sqrt{N}$, $[\sqrt{m}]$	2.0	4.8
Absolute (room) temperature, Θ, [K]	298	

2.4 PINN implementation

The PINN architecture adopted here has been presented by [8] and is illustrated in Fig. 2. It entails ANN's that are trained to solve the kinematic conditions alongside with the constitutive law. Two main steps are undertaken for its implementation. First, the strong form (boundary valued equation system, formed by the Dirichlet, Neumann and contact conditions) is applied to the spatial gradients of the primary variable as the physical constraint. Second, the energy form (obtained from the weak form) is applied to the primary variable as an additional constraint for training. This approach only requires first-order derivatives to construct the physical loss functions, which reduces the computational cost and improves accuracy.

Approximately 100 collocation points is used in each problem configuration and the number of epochs for the training was kept at 1000. Three hidden layers are employed, each one with 400 neurons.

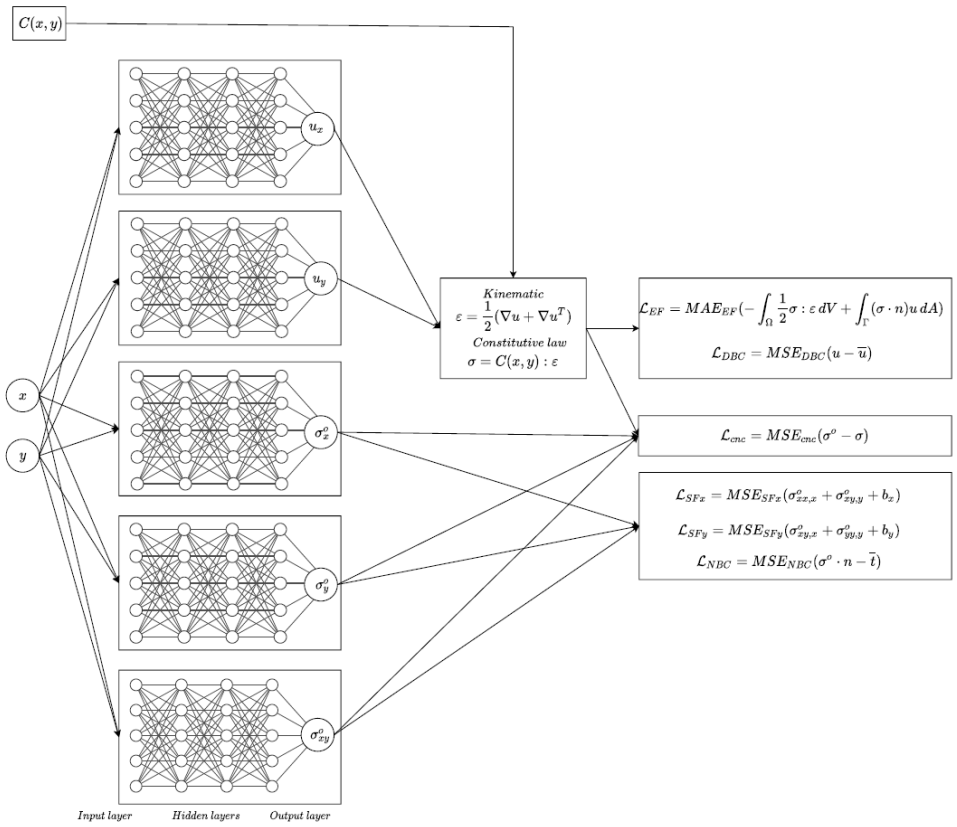

Figure 2. Architecture and loss functions, retrieved from [8].

3 Results and Discussion

The simulations showed accurate representations of nodal displacement, reaction forces and stress-strain behavior for both PLA and ABS. Fig. 3 and Fig. 4 depicts representative results of the conditions analyzed. The stress-strain behavior observed in both tests show a similar trait: they contain an elastic zone and an inelastic zone that can be represented by a linear trendline with a coefficient of determination over 97 %. Moreover, they both presented a typical transition zone due to yielding and hardening. On one hand, the tensile results in the transition zone are smooth and could be easily described by a third-order polynomial equation. On the other hand, the transition zone of the indentation tests is irregular and computationally challenging for all methods tested.

In terms of accuracy, all methods show a close representation of the physical behavior observed during the experimental tests. For instance, the maximum stresses observed on ABS specimens at tensile and indentation are: experimental data, 31.97 MPa and 54.71; Mullliken-Boyce, 31.93 MPa and 55.60 MPa; Pupure et al, 31.95 MPa and 54.61 MPa; PINN, 31.96 MPa and 54.80 MPa. To be specific, the highest relative error noticed for a stress/strain assessment are equal to 4.1% for the PLA and 3.9% for the ABS. Moreover, these values are observed in transition zone (region with the highest level of nonlinearity). Since the experimental procedures also have their own sources of uncertainty (e.g. specimen's dimensional deviation and load cell registry errors), the errors observed can be regarded as negligible.

4 Conclusions

The main advantages of the PINN studied in this work is the simplicity of its implementation and fast solution (centiseconds) when fully trained. However, the training time required for the calibration of the PINNs is a major drawback. The FE simulations were run in a DELL T-7910 workstation (02 Intel® Xeon® E5-2630 v3 with 8 Cores at 3.2 GHz and 20 Mb cache; and 196 GB of available RAM). Although the development of FE models and VUMAT subroutines took around 12h each, the solution of the tensile and the indentation problems took only 1 min 52 s and 2 min and 46 s, respectively. The computational time for the ABS and PLA were almost

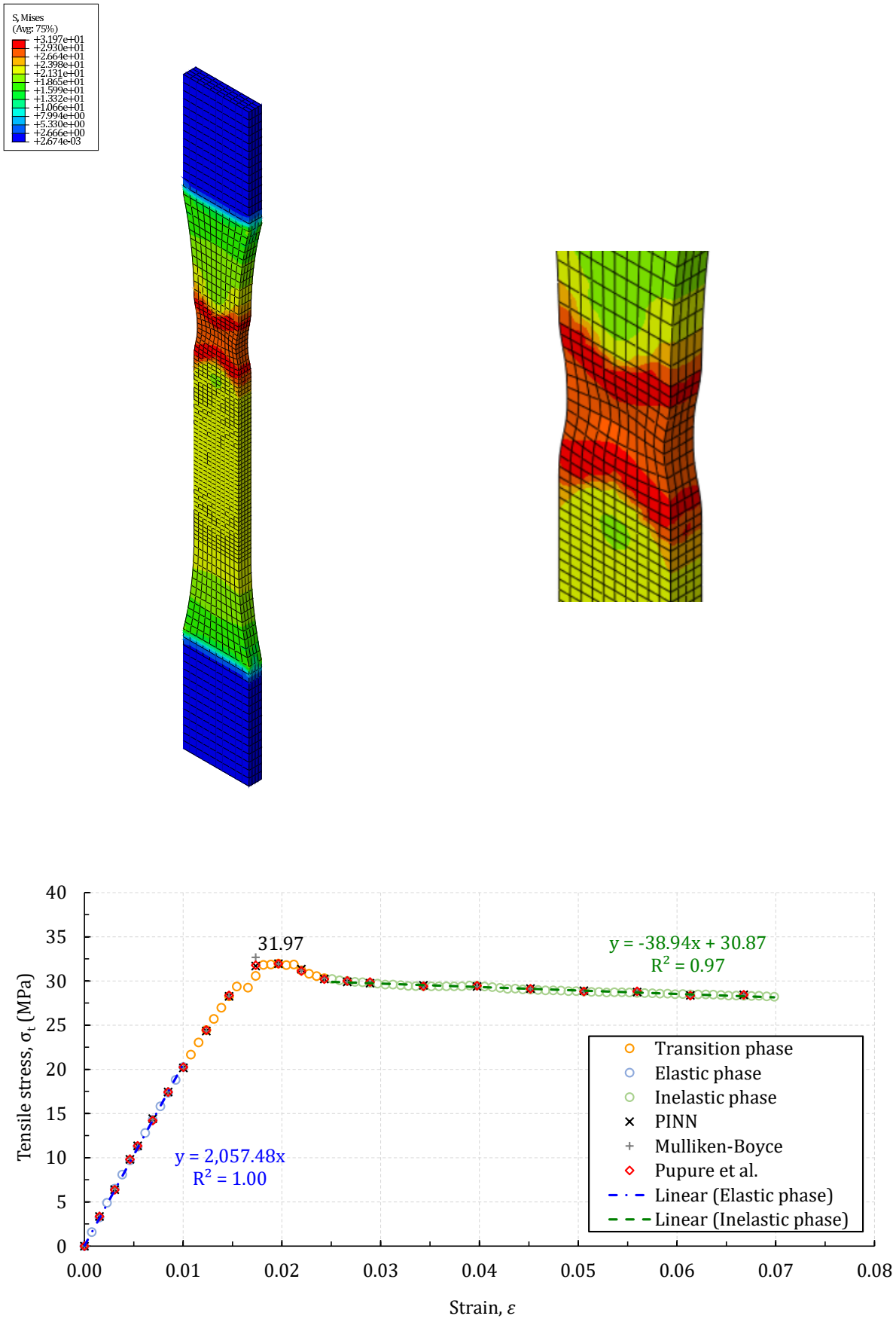

Figure 3. ABS tensile results: finite element stress distribution (max stress of 31.97 MPa at 4 mm displacement / 0.017 strain), close up of the damage zone and stress-strain behavior.

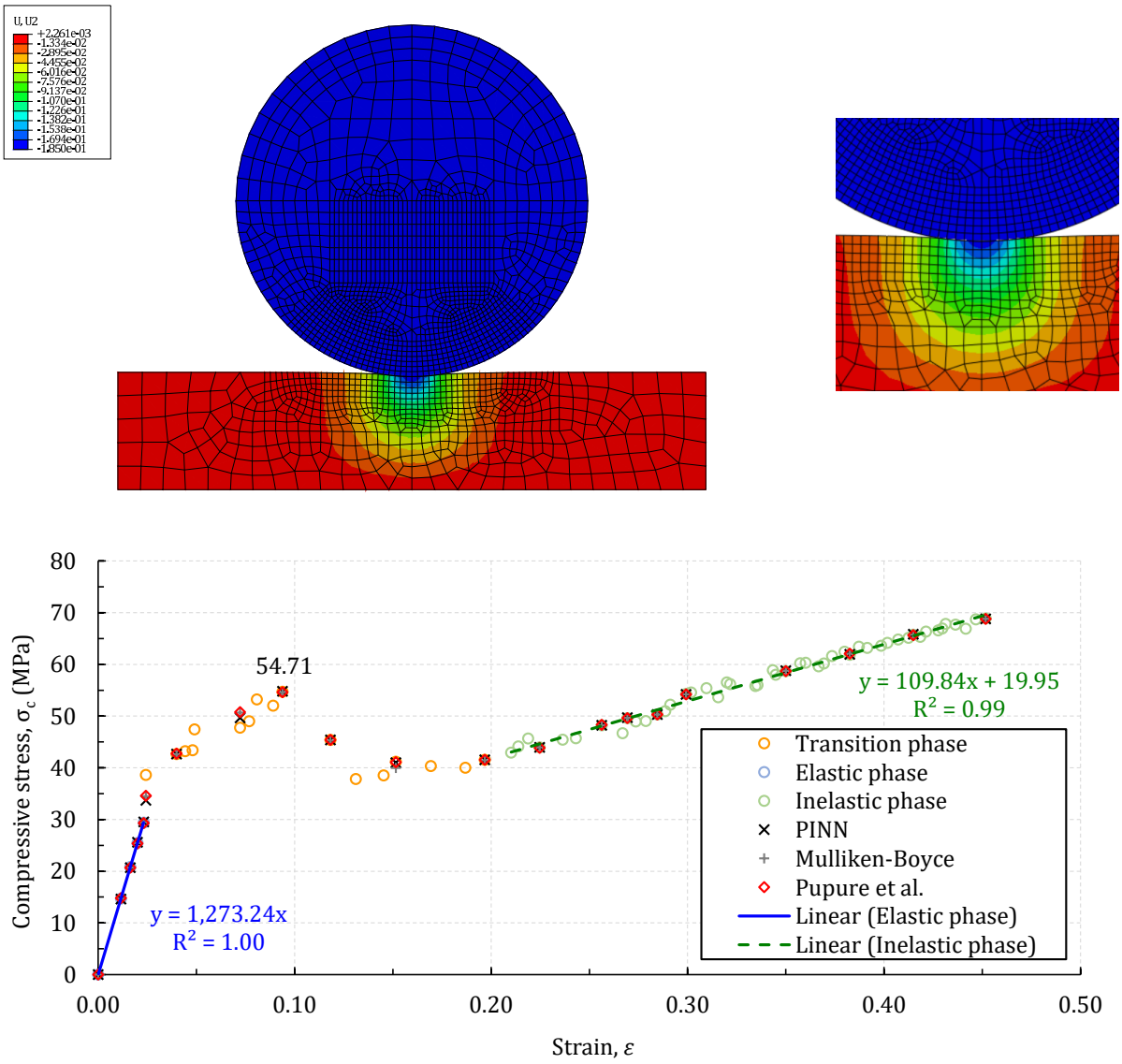

Figure 4. ABS indentation results: finite element displacement distribution (max indentation of 1.85 mm / 0.44 strain), close up of the damage zone and stress-strain behavior.

identical. Meanwhile, the implementation of the PINN took around 48h and its training process took almost a month (continuous real time). Therefore, unless the PINN's are a part of broader strategy – such as the analysis of several types of loading conditions in order to determine behavioral trends – its cost might be unreasonable. In particular, the use of PINNs for the analysis of time dependent phenomena such as creep and fretting wear might be an efficient approach and we aim to explore it soon.

Acknowledgements. The authors gratefully acknowledge the financial support provided by the Brazilian National Council for Scientific and Technological Development (CNPq), the Brazilian Federal Agency for Support and Evaluation of Graduate Education (CAPES) and the Foundation for the Support of Research in the Federal District (FAP-DF).

Authorship statement. The authors hereby confirm that they are the sole liable persons responsible for the authorship of this work, and that all material that has been herein included as part of the present paper is either the property (and authorship) of the authors, or has the permission of the owners to be included here.

References

[1] A. Tiwari, N. Murugan, and R. Ahuja. *Advanced Engineering Materials and Modeling*. Wiley, 2016.
[2] T. Doca and F. Andrade Pires. Analysis of a cylinder-to-flat contact problem at finite elasto-plastic strains. *Tribology International*, vol. 79, pp. 92–98, 2014.
[3] T. Doca and F. Andrade Pires. Finite element modeling of wear using the dissipated energy method coupled with a dual mortar contact formulation. *Computers and Structures*, vol. 191, pp. 62–79, 2017.
[4] T. Doca, F. Loyola, and E. Albuquerque. Numerical frameworks for fretting fatigue life analysis: Modeling, validation and experimental comparison. *Theoretical and Applied Fracture Mechanics*, vol. 121, n. 103479, 2022.
[5] R. Guedes (ed.). *Creep and fatigue in polymer matrix composites.* UK: Woodhead Publishing Materials, 2011.
[6] M. Raissi, P. Perdikaris, and G. Karniadakis. Physics-informed neural networks: A deep learning framework for solving forward and inverse problems involving nonlinear partial differential equations. *Journal of Computational Physics*, vol. 378, pp. 686–707, 2019.
[7] M. Fernández, M. Jamshidian, T. Böhlke, K. Kersting, and O. Weeger. Anisotropic hyperelastic constitutive models for finite deformations combining material theory and data-driven approaches with application to cubic lattice metamaterials. *Computational Mechanics*, vol. 67, pp. 653–677, 2021.
[8] S. Rezaei, A. Harandi, A. Moeineddin, B. Xu, and S. Reese. A mixed formulation for physics-informed neural networks as a potential solver for engineering problems in heterogeneous domains: Comparison with finite element method. *Computer Methods in Applied Mechanics and Engineering*, vol. 401, n. 115616, 2022.
[9] *ASTM 638-14 Standard Test Method for Tensile Properties of Plastics*. ASTM International, 2021.
[10] M. Wang, J. Wu, Y. Hui, Z. Zhang, X. Zhan, and R. Guo. Identification of elastic-plastic properties of metal materials by using the residual imprint of spherical indentation. *Materials Science and Engineering*, vol. 679, pp. 143–154, 2017.
[11] A. Bhat and R. New. An improved methodology for extracting uniaxial stress–strain curves from spherical indentation data. *Mechanics of Materials*, vol. 174, n. 104459, 2022.
[12] T. Pandim, K. Sales de Oliveira, J. Araújo, F. Andrade Pires, and T. Doca. Indentation, creep and axial–torsional fretting wear analysis of PC/ABS blends. *Tribology International*, vol. 188, n. 108763, 2023.
[13] R. Leão, L. Jesus, P. Bertuoli, A. Zattera, J. Maia, C. del Menezzi, S. Amico, and S. da Luz. Production and characterization of cellulose nanocrystals / acrylonitrile butadiene styrene nanocomposites. *Journal of Composite Materials*, vol. 0, n. 0, pp. 1–8, 2020.
[14] L. Jesus, J. Oliveira, R. Leão, L. Beltrami, A. Zattera, C. Anflor, T. Doca, and S. da Luz. Tensile behavior analysis combined with digital image correlation and mechanical and thermal properties of microfibrillated cellulose fiber/polylactic acid composites. *Polymer Testing*, vol. 113, n. 107665, 2022.
[15] A. Mulliken and M. Boyce. Mechanics of the rate-dependent elastic–plastic deformation of glassy polymers from low to high strain rates. *International Journal of Solids and Structures*, vol. 43, pp. 1331–1356, 2006.
[16] L. Zapas and J. Crissman. Creep and recovery behavior of ultra-high molecular weight polyethylene in the region of small uniaxial deformations. *Polymer*, vol. 25, pp. 57–62, 1984.
[17] L. Pupure, J. Varna, and R. Joffe. Natural fiber composite: Challenges simulating inelastic response in strain-controlled tensile tests. *Journal of Composite Materials*, vol. 50, n. 5, pp. 575–587, 2016.